RESEARCH PAPER

Channels 10:1, 55–68; January/February 2016; © 2016 Taylor & Francis Group, LLC

Interactions between N and C termini of α_{1C} subunit regulate inactivation of $Ca_V1.2$ L-type Ca^{2+} channel

Adva Benmocha Guggenheimer[1,2], Lior Almagor[2,3,#], Vladimir Tsemakhovich[1,#], Debi Ranjan Tripathy[3], Joel A Hirsch[3], and Nathan Dascal[1,*]

[1]Department of Physiology and Pharmacology; Sackler School of Medicine; Sagol School of Neuroscience; Tel Aviv, Israel; [2]Present address: Department of Structural Biology, Stanford University, School of Medicine; Stanford, CA USA; [3]Department of Biochemistry & Molecular Biology; Institute of Structural Biology, George S. Weiss Faculty of Life Sciences; Sagol School of Neuroscience; Tel Aviv University; Tel Aviv, Israel

[#]These authors contributed equally to this work.

Keywords: binding, calcium channel, calmodulin, C-terminus, $Ca_V1.2$, inactivation, L-type, N-terminus

The modulation and regulation of voltage-gated Ca^{2+} channels is affected by the pore-forming segments, the cytosolic parts of the channel, and interacting intracellular proteins. In this study we demonstrate a direct physical interaction between the N terminus (NT) and C terminus (CT) of the main subunit of the L-type Ca^{2+} channel $Ca_V1.2$, α_{1C}, and explore the importance of this interaction for the regulation of the channel. We used biochemistry to measure the strength of the interaction and to map the location of the interaction sites, and electrophysiology to investigate the functional impact of the interaction. We show that the full-length NT (amino acids 1-154) and the proximal (close to the plasma membrane) part of the CT, pCT (amino acids 1508-1669) interact with sub-micromolar to low-micromolar affinity. Calmodulin (CaM) is not essential for the binding. The results further suggest that the NT-CT interaction regulates the channel's inactivation, and that Ca^{2+}, presumably through binding to calmodulin (CaM), reduces the strength of NT-CT interaction. We propose a molecular mechanism in which NT and CT of the channel serve as levers whose movements regulate inactivation by promoting changes in the transmembrane core of the channel via S1 (NT) or S6 (pCT) segments of domains I and IV, accordingly, and not as a kind of pore blocker. We hypothesize that Ca^{2+}-CaM-induced changes in NT-CT interaction may, in part, underlie the acceleration of $Ca_V1.2$ inactivation induced by Ca^{2+} entry into the cell.

Introduction

Intracellular Ca^{2+} concentration is maintained at very low levels under resting conditions, below 100 nM. [1] However, it rises sharply (to tens or hundreds of μM within channel's nanodomain) [2] upon stimulation. The principal Ca^{2+} entryways of nerve, muscle, and some endocrine cells are VGCCs (voltage-gated Ca^{2+} channels). Because Ca^{2+} ions are chemical messengers, [1] influx through VGCCs can directly link membrane potential changes to stimulation of intracellular signaling cascades.[3] Since excess Ca^{2+} influx is toxic, Ca^{2+} entry into the cell is tightly regulated. Hence, VGCC activity is controlled by self-regulatory and extrinsic mechanisms that tune their action. Inactivation, i.e. loss of conductance during stimulation, is an important negative feedback mechanism in which VGCCs are regulated by entering Ca^{2+} and internal Ca^{2+} levels (Ca^{2+}-dependent inactivation) and by conformational changes induced by the membrane potential (voltage-dependent inactivation).[4] Channel inactivation generates short and accurate Ca^{2+} signals, which prevent high toxic levels of Ca^{2+}. Visionary studies of David Yue and collaborators, and of other research groups, revealed the crucial role of VGCC cytosolic domains and calmodulin (CaM) in the process of inactivation, and provided formidable quantitative and qualitative information about this complex machinery. Nonetheless, many details of the molecular mechanisms of inactivation remain incompletely understood.

The main subunit of the ubiquitous L-type VGCC $Ca_V1.2$, α_{1C}, has cytosolic amino and carboxyl termini (NT and CT) (**Fig. 1**). NT and CT play an important role in the inactivation of the channel, and in gating in general. The pCT contains EF hand, preIQ and IQ motifs, and is necessary for Ca^{2+}-dependent inactivation, Ca^{2+}-dependent facilitation and voltage-dependent inactivation.[5-8] Deletion of the NT results in changes of the inactivation properties of the channel.[9] Truncation of a major part of both termini from the pore forming α_{1C} subunit causes changes in the properties of the current of the channel,[4,10-12] which are more than additive compared to changes caused by each truncation.[10]

*Correspondence to: Nathan Dascal; Email: dascaln@tauex.tau.ac.il
Submitted: 04/28/2015; Revised: 09/28/2015; Accepted: 10/11/2015
http://dx.doi.org/10.1080/19336950.2015.1108499

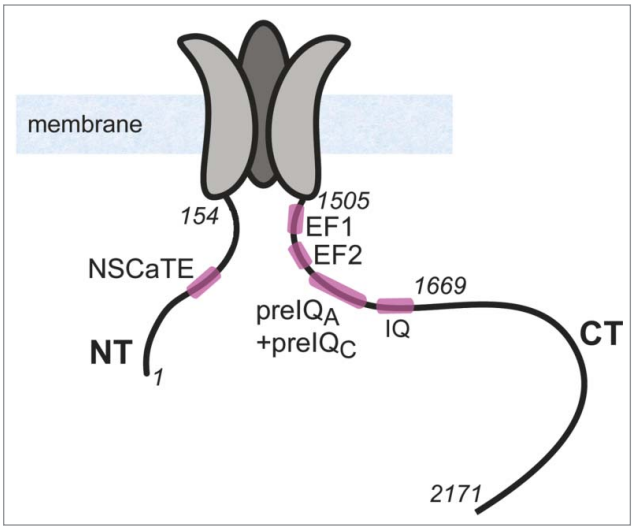

Figure 1. Illustration of the structure of α_{1C} subunit of $Ca_V1.2$. NT and CT and 3 out of the 4 transmembrane domains of α_{1C} are shown schematically. Cytosolic loops I, II and III are not shown. In italics are numbers of selected a.a. residues in NT and CT, shown for orientation.

CaM is a small (148 amino acids (a.a.), 17 kDa), soluble, Ca^{2+}-binding protein with N-terminal and C-terminal lobes ($CaM_{N\text{-}lobe}$ and $CaM_{C\text{-}lobe}$, respectively). Its flexible structure enables CaM to serve as a Ca^{2+} sensor for a wide range of target proteins of various structures involved in a wide array of functions in the cell.[8,13-15] Ca^{2+} binding to CaM induces a conformational change in CaM, in turn altering either the association with target proteins or the tertiary structure of the CaM:target complex, thus transforming changes of intracellular Ca^{2+} levels into modulation of function.[16-18] A number of regulatory mechanisms of $Ca_V1.2$ by CaM have been proposed, all of which utilize its plasticity in interacting with its target proteins. CaM has several interaction sites on $Ca_V1.2$ (**Fig. 1**). In the CT, they comprise the IQ motif, essential for CaM regulation of $Ca_V1.2$, [19-22] and the PreIQ, which contains 2 potential Ca^{2+}-CaM binding sites known as $preIQ_A$ and $preIQ_C$.[23-25] The NT contains the NSCaTE motif,[4,10] a short linear segment in the NT found only in the $Ca_V1.2$ and $Ca_V1.3$ L-type Ca^{2+} channels (a.a. 82-90, numbering by rabbit cardiac α_{1C}). CaM binds NSCaTE in a Ca^{2+}-dependent manner[10] and undergoes a significant structural change, from unstructured to α-helix upon binding CaM.[26,27]

The $Ca_V1.2$ NT and CT play an important role in gating. They have been the subject of many studies which demonstrated how various NT and pCT deletions and mutations dramatically change inactivation.[6,9-11,28-34] It has been proposed that, following channel opening and Ca^{2+} entry, the previously CT-anchored and now Ca^{2+}-bound CaM binds the NSCaTE, bridging the NT and CT, tightening an "NT-CT scaffold"[10] and promoting the inactivation process.[4] However, this attractive hypothesis lacks direct proof, and has been challenged by the finding that Ca^{2+}-bound CaM does not foster a direct binding between the NSCaTE and the CT.[35] We, therefore, sought evidence for a CaM-independent interaction between the NT and CT. Our data indicate that the 2 cytosolic segments indeed interact directly, possibly affecting inactivation. Furthermore, Ca^{2+}-CaM alters the NT-CT interaction, providing a new insight into the underlying mechanism and leading us to suggest revisions to previously proposed models.[4,10]

Results

NT-pCT interaction

The inactivation of the $Ca_V1.2$ channel involves different parts of the channel. We focused on the role of the cytosolic parts of the channel, and the NT ($NT_{1\text{-}154}$) and pCT ($pCT_{1505\text{-}1671}$) of the α_{1C} subunit in particular (**Fig. 1**). We first performed pull-down assays in order to test for potential interactions. We synthesized ^{35}S-labeled $pCT_{1505\text{-}1671}$ proteins (target) *in vitro* in reticulocyte lysate and pulled them down with GST-$NT_{1\text{-}154}$ protein (bait). We note that the reticulocyte lysate undoubtedly contains intrinsic CaM, but its amount relative to the newly synthesized protein could not be estimated.

The results revealed a Ca^{2+}-regulated interaction between the NT and pCT (**Fig. 2**). The robust NT-pCT interaction observed in a Ca^{2+}-free buffer was reduced in the presence of a high level of Ca^{2+} (1 mM, **Fig. 2**, right) but not in the presence of a lower Ca^{2+} concentration (0.2 mM, **Fig. 2**, left). However, in the presence of purified CaM, the interaction was reduced by both 0.2

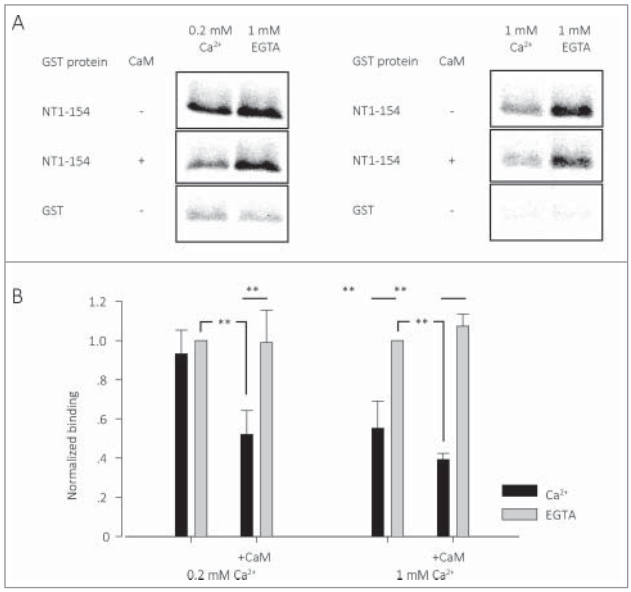

Figure 2. $CT_{1505\text{-}1671}$ (IVT) interaction with GST-$NT_{1\text{-}154}$ in the presence of Ca^{2+} or EGTA, with or without CaM. (**A**) Pull down experiment of radioactively labeled pCTs, pulled by GST-$NT_{1\text{-}154}$. Radiograms of the labeled proteins are shown. (**B**) Average of 4-6 pull down experiments as in A. Each group of experiments is normalized to the conditions of EGTA with no CaM of the same group. 0.2 mM was calculated with the winmaxc32 software. ** $p < 0.01$. All the experiments were done with 3 μg GST-$NT_{1\text{-}154}$ and CaM.

and 1 mM Ca^{2+}. These results indicate the possibility of a Ca^{2+}/CaM-dependent weakening of the NT-pCT interaction upon physiologically relevant Ca^{2+} increase within the channel nanodomain. Without the added CaM, the endogenous CaM derived from the reticulocyte lysate was probably insufficient to saturate all the overexpressed pCT, and this probably explains the inability of 200 μM Ca^{2+} to significantly reduce the observed NT-pCT binding.

To confirm and quantitate the NT-pCT interaction, we used recombinant purified proteins. pCT expressed in E. coli separately or in the presence of CaM was unstable at low Ca^{2+} concentrations (data not shown, and see below). We engineered a construct in which CaM was fused to the C-terminal end of pCT separated by a 14 a.a. residue linker (**Fig. 3A** and Methods). A mutant C1564S $pCT_{1508-1669}$ was used in order to generate a protein containing a single Cys for the labeling (CaM sequence does not contain Cys residues). This protein, termed $pCT_{1508-1669}$(C1564S)-lnk-CaM, was stable at all Ca^{2+} concentrations. As the interaction partner, we used the full NT (MBP-NT_{1-154}) and NT segments as a fusion to maltose binding protein (MBP). This fusion facilitates protein expression and stability. All MBP-fused proteins also contained a His-tag (**Fig. 3A**).

Interaction between MBP-NT_{1-154} and $pCT_{1508-1669}$(C1564S)-lnk-CaM was studied using microscale thermophoresis (MST), at Ca^{2+} concentrations between 0 to 1 mM. In the virtual absence of free Ca^{2+} (1 mM EDTA), the MST signal showed a monophasic binding curve with a dissociation constant (K_D) of 0.72 μM (**Fig. 3B**). For all Ca^{2+} concentrations tested except 1 mM, monophasic binding curves were obtained. The K_D mildly increased (pointing at a decrease in the affinity of interaction) until levelling off at 3-4 μM between 10 and 100 μM Ca^{2+} (**Fig. 3C, 3F**). At 1 mM Ca^{2+} a biphasic MST signal curve was obtained (**Fig. 3D**), with a descending high-affinity component (apparent K_D of ~0.2 μM) and an ascending component, like at all other Ca^{2+} concentrations, of lower affinity (K_D = 4.34 μM; **Fig. 2E**). Whereas the interpretation of the high-affinity component of binding seen at 1 mM Ca^{2+} is unclear, it can be safely stated that in the physiologically relevant Ca^{2+} range, NT and CaM-fused CT associate with sub-micromolar to low micromolar affinity, which weakens as Ca^{2+} concentration rises (**Fig. 3F**).

We also pursued characterization of NT-CT interactions using pCT constructs bacterially coexpressed with CaM rather than as a fusion protein. We prepared His-tagged $pCT_{1508-1669}$ ($Ca_V1.2$ CT a.a. 1508-1669) containing the

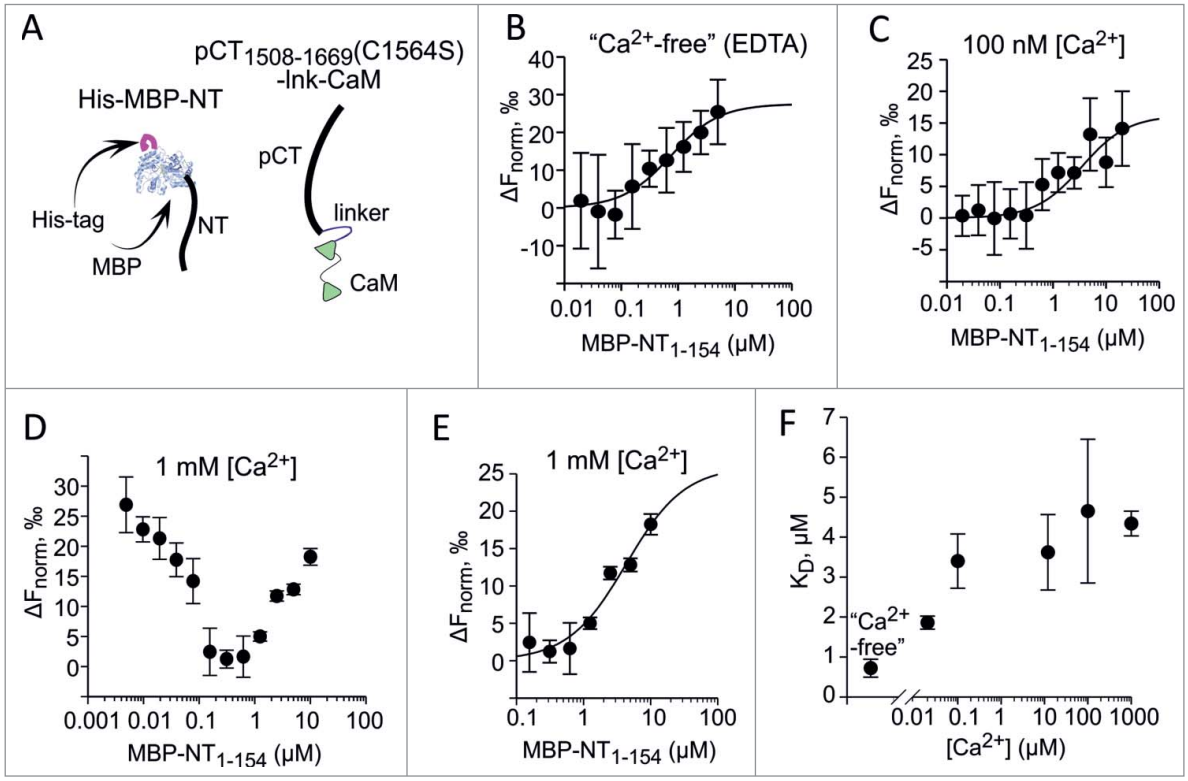

Figure 3. Interaction between $pCT_{1508-1669}$(C1564S)-lnk-CaM with MBP-NT_{1-154} studied by MST. MST monitoring of the interaction was done by titrating labeled $pCT_{1508-1669}$(C1564S)-lnk-CaM (50 nM) with increasing doses of MBP-NT_{1-154}. Each individual data point shows mean±SEM from 2-3 independent determinations. The Ca^{2+} concentration was adjusted using EDTA and $CaCl_2$ (for 100 μM, 12 μM, 100 nM and 20 nM) at 25° C. The binding curves in B, C and E were fitted to data using the Monolith software. (**A**) Schematic presentation of the proteins used. (**B**) Titrating MBP-NT_{1-154} in virtual absence of Ca^{2+}. The binding buffer contained 1 mM EDTA and no added Ca^{2+}. (**C**) Titrating MBP-NT_{1-154} at 100 nM Ca^{2+}. (**D**) Titrating MBP-NT_{1-154} at 1 mM Ca^{2+}. The raw data shown indicate a biphasic event. (**E**) For 1 mM Ca^{2+}, the K_D of the low-affinity phase (4340 ± 309 nM) was determined from the fitting of data for MBP-NT_{1-154} concentrations above 0.1 μM. The high-affinity phase yields a K_D of 41.2 ± 4.4 nM (fit not shown). (**F**) Ca^{2+}-dependent changes in K_D of $pCT_{1508-1669}$(C1564S)-lnk-CaM with MBP-NT_{1-154} interaction. For 1 mM Ca^{2+}, only the low-affinity K_D point is shown.

C1564S mutation and coexpressed it with CaM in *E. coli*. $pCT_{1508-1669}$ co-purifies with CaM on both Ni^{2+} chelation and gel-filtration columns (see Methods), as a $pCT_{1508-1669}$/CaM complex. Nevertheless, this protein complex tends to precipitate at low Ca^{2+} concentrations, therefore, all experiments were performed at 1 mM Ca^{2+}.

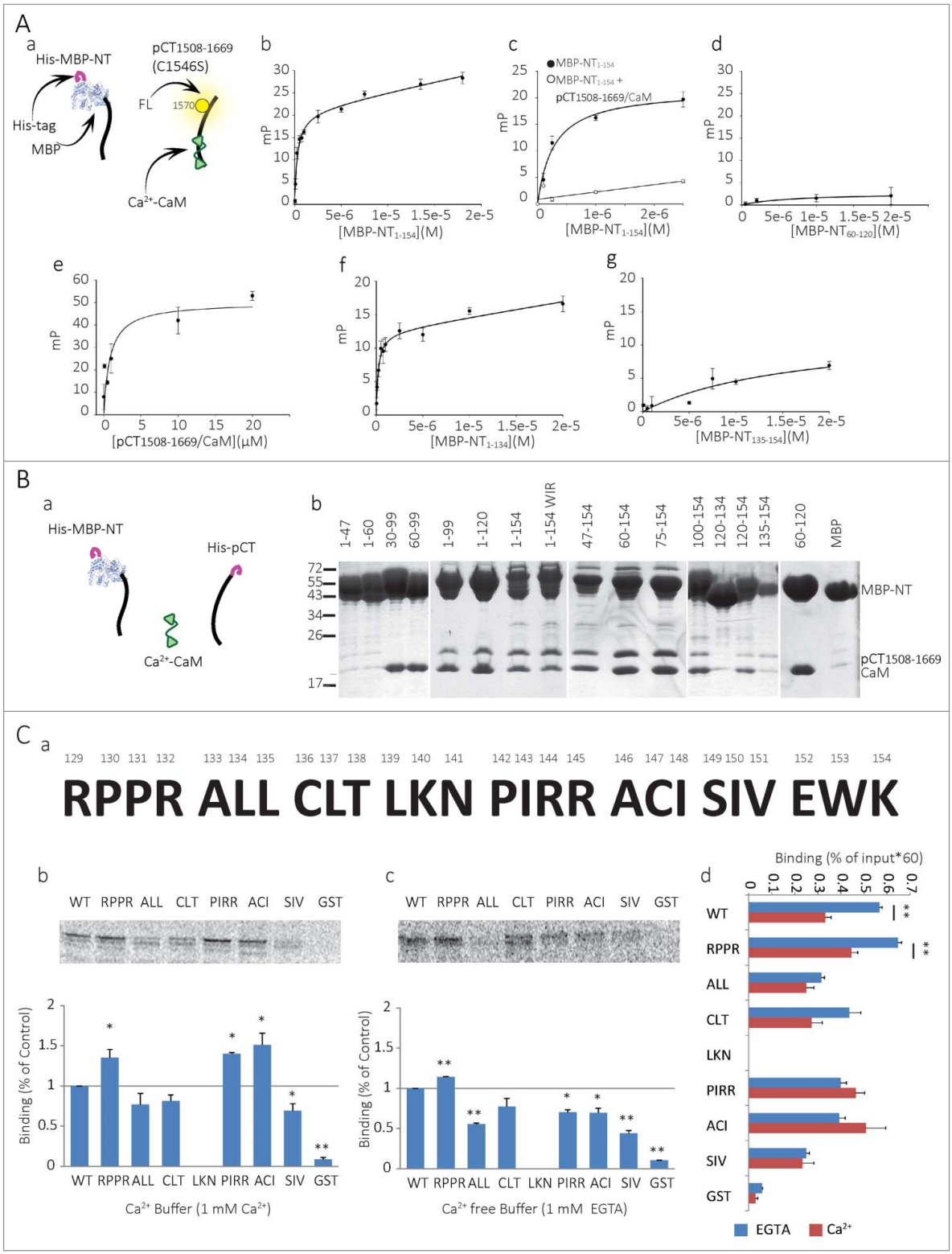

Figure 4. For figure leend, see page 59.

To further quantitate the NT-CT interaction and map the important sites using the $pCT_{1508-1669}$/CaM complex, we employed a fluorescence-based binding assay (**Fig. 4A**). A fluorescent $pCT_{1508-1669}$ was produced by chemically conjugating a fluorescein to the C1570 thiol group of $pCT_{1508-1669}$. Both C1564 and C1570 are located in $pCT_{1508-1669}$'s predicted EF-hand helix bundle, but are not part of the putative Ca^{2+}- or Mg^{2+}- binding positions.[36] Binding of the NT to the $pCT_{1508-1669}$/CaM complex was assessed using fluorescence polarization (FP) measurements at the fluorescein emission peak. The dependence of FP on molecular mobility enables accurate measurement of the binding of a fluorescent group to another molecular entity which, when associated, form a larger fluorescent complex.

The FP assay also demonstrates the interaction between NT and pCT. The binding curve of the fluorescein-labeled $pCT_{1508-1669}$/CaM and MBP-NT_{1-154} was monophasic with $K_D = 0.29 \pm 0.05$ μM (**Fig. 4Ab**). When excess unlabeled $pCT_{1508-1669}$/CaM was added, the FP returned to baseline, proving the interaction to be specific (**Fig. 4Ac**). The apparently higher interaction affinity and the absence of 2 binding phases, as compared to the MST data in 1 mM Ca^{2+}, may stem from the use of different methods and protein constructs (fused vs. non-fused CaM). Nonetheless, both methods provide clear evidence for a submicromolar to low-micromolar affinity interaction between NT and pCT/CaM, even in high Ca^{2+}.

Mapping the sites of NT-pCT-CaM interaction

We mapped the location of the NT-CT binding determinants using the FP assay with pCT/CaM and MBP-fused segments of the NT. As observed in **Figure 4A**d, MBP-NT_{60-120}, which includes the NT CaM-binding site, NSCaTE, did not bind the $pCT_{1508-1669}$/CaM complex. This finding is not consistent with a previous proposal that Ca^{2+}-CaM may be the bridging element between the NT and CT of the channel, binding with its C-lobe to the CT IQ domain and with its N-lobe to the NT CaM binding site. [4] In addition, this result rules out a possible interaction between pCT and the MBP moiety of the tested NT fragments.

Figure 4Ae shows a FP assay in an inverse configuration, where NT segment lacking the first 46 a.a., NT_{47-154}(C136S), was titrated by pCT/CaM (Cys136 in the NT was mutated to Ser leaving only one thiol group in NT, in C147). This truncated NT bound unlabeled $pCT_{1508-1669}$/CaM with a K_D of 0.85± 0.37 μM, indicating that the first 46 a.a. of the NT are not essential for the NT-CT interaction. Further FP assays with fluorescein-labeled $pCT_{1508-1669}$/CaM explored the role of the last 20 a.a. of NT (residues 135-154) which appeared functionally important for the inactivation process (see below). Deletion of this region has little effect on NT-pCT binding ($K_D = 0.21 \pm 0.06$ μM for MBP-NT_{1-134}, Fig 4Af). Nevertheless, the MBP-fused $NT_{135-154}$ alone bound $pCT_{1508-1669}$/CaM albeit with a much lower apparent affinity ($K_D = 16.67 \pm 28.58$ μM, **Fig. 4Ag**). Thus, the last 20 amino acids of the $NT_{135-154}$, are sufficient for binding the pCT and may participate in NT-CT binding, but do not constitute the only or the major binding determinant, at least under high-Ca^{2+} conditions. The low affinity of interaction may also indicate that the construct used lacked additional amino acid residues, located N-terminally to the last 20 a.a., which may constitute a part of the binding site (see below).

In order to further map the $Ca_V1.2$ NT-pCT interaction sites, a pull down analysis was performed (**Fig. 4B**). $pCT_{1508-1669}$ and CaM were co-expressed together with a particular MBP-fused NT truncation in *E.coli* (**Fig. 4Ba**). The interaction with the NT was detected using pulldown with amylose resin in the presence of 1 mM Ca^{2+}. The experiments were performed in 2 steps. For the first step, both the pCT and MBP-NT proteins were pulled down using a Ni^{2+}-chelate resin, as both proteins contained His-tags. Subsequently, the eluted proteins were incubated with amylose beads which pull-down only the MBP-NT moiety. Since CaM is tag-less, it was pulled down via the NSCaTE-containing segments of NT or via its interactions with the pCT. Pull-down results (**Fig. 4Bb**) showed ternary NT-pCT-CaM complex formation for MBP-NT_{1-154}, whereas no binding of pCT/CaM was observed for the MBP control. The results also demonstrate that the shortest segment that successfully pulled down pCT is $NT_{135-154}$. MBP-NT_{60-120}, MBP-NT_{30-99} and MBP-NT_{60-99}, the NSCaTE-containing segments,[4] also did not bind to pCT but, as expected, pulled-down CaM by direct binding. In addition, binding was observed for NT with a triple 'WIR' mutation (W82A, I86A and R90A), previously shown to abrogate CaM binding to NSCaTE.[4,35] These results are in full agreement with the FP mapping. First, they again prove that NSCaTE does not take part in the NT-pCT interaction. Second, they confirm that the 135-154 a.a. segment is sufficient to bind pCT/CaM. Moreover, they underscore the importance of this segment (despite the apparently low affinity seen in direct FP assay), and hint that

Figure 4 (See previous page). The NT-pCT interaction site in the NT. (**A**) Binding isotherms of $Ca_V1.2$ MBP-NT proteins with a fluorescein-labeled $pCT_{1508-1669}$/CaM complex measured by fluorescence polarization (FP). **a.** Schematic illustration of the fluorescein labeled 'bait' and MBP fused 'target' molecules used in the assay (label is on $pCT_{1508-1669}$ C1570). **b.** Full length MBP-NT_{1-154} binds $pCT_{1508-1669}$ with $K_D = 0.29 \pm 0.05$ μM. **c.** MBP-NT_{1-154} binding is specific to $pCT_{1508-1669}$/CaM. FP signal is abolished with the addition of excess unlabeled ('cold') $pCT_{1508-1669}$/CaM (5 μM, 100 fold higher than labeled protein). **d.** No binding was observed for MBP-NT_{60-120}. **e.** Binding is also observed for a converse FP experiment where a fluorescein labeled NT_{47-154}(C136S) is titrated with the $pCT_{1508-1669}$/CaM complex. **f.** MBP-NT_{1-134} binds $pCT_{1508-1669}$/CaM with $K_D = 0.21 \pm 0.06$ μM. **g.** MBP-$NT_{135-154}$ only weakly binds $pCT_{1508-1669}$/CaM with $K_D = 16.67 \pm 28.58$ μM. All measurements were performed at 10° C. Solutions contained 1 mM $CaCl_2$ and 25% glycerol. Fitting model assumed a single binding site + non-specific binding. mP denotes the change from baseline (ΔP) polarization in thousandth FP unit. (**B**) Pull-down experiment of $pCT_{1508-1669}$ and CaM by MBP-fused NT fragments. **a.** Schematic illustration of the proteins used: His-MBP-NTs, CaM and His-pCT. **b.** Final elution from amylose resin used for immobilization is presented. (**C**) **a.** NT 129-154 mutations arranged in triples or quadruples which were mutated to alanines. **b-c. Top**, pull down experiments of radioactive labeled NTs, pulled by GST-pCT in 1 mM Ca^{2+} (**b**) or 1 mM EGTA (**c**). Bottom, average of 3 of pull down experiments normalized to WT NT of each experiment. * $P < 0.05$, ** $P < 0.01$. **d.** Non-normalized average of 3 pull down experiments with EGTA (blue bars) or 1 mM Ca^{2+} (dark red bars). ** $P < 0.01$.

there are multiple structural determinants on the NT, skirting NSCaTE, that participate in the interaction with the CT. Binding of $pCT_{1508-1669}$ was observed for MBP-NT_{1-120} and MBP-NT_{60-154} but not for MBP-NT_{60-120}. These results imply a complex arrangement of NT. Certain NT-pCT binding determinants are located both within NT_{1-47} and $NT_{135-154}$, and possibly in additional parts of the NT.

Studying the role of NT segment proximal to the plasma membrane by mutagenesis

Next, we mutated a.a. triplets or quadruplets to alanine in NT_{1-154}, covering residues 129-154, in order to locate critical a.a. within this segment pivotal for interaction with pCT (**Fig. 4Ca**). We used pull-down assays to pull mutated [S^{35}]-Met labeled NT_{1-154} with GST-pCT/CaM in the presence of 1 mM Ca^{2+} (high Ca^{2+}) or 1 mM EGTA (Ca^{2+}-free). For the GST-pCT/CaM production, we co-expressed GST-pCT in *E. coli* with CaM; CaM remains bound to the pCT in the production process. The changes in interaction caused by the alanine mutations are different in high Ca^{2+} and Ca^{2+}-free buffers. Under high Ca^{2+} conditions, mutated NT_{1-154}RPPR (a.a. 129-132), NT_{1-154}PIRR (a.a. 142-145) and NT_{1-154}ACI (a.a 146-148) significantly increased the NT-pCT interaction (**Fig. 4Cb**). In contrast, under Ca^{2+}-free conditions, all mutations except NT_{1-154}RPPR and NT_{1-154}CLT reduced the NT-pCT interaction (**Fig. 4Cc**). These results suggest that the part of NT close to the plasma membrane contributes to NT-CT binding under low-Ca^{2+} conditions. This segment, which we provisionally term "the proximal NT," or pNT, comprises the last 20 a.a. of the NT explored in the FP and pulldown assays, probably together with a few preceding residues, in particular A133 and L134. Since most pNT mutations reduce NT-pCT/CaM interaction in low Ca^{2+} but not in high-Ca^{2+} (where some mutations even improve the binding), it is plausible that the affinity of pNT to pCT/CaM is higher in low-Ca^{2+} than in high-Ca^{2+}. This may in part underlie the apparent low affinity of pCT interaction with the last 20 a.a. of NT observed in the FP assay in the presence of high-Ca^{2+}.

Full analysis of pull-down results for all mutations is shown in **Fig. 4Cd**. For each radioactively labeled NT_{1-154} protein, binding is shown as % of input (not normalized to any standard group). These results confirm that high Ca^{2+} reduces the interaction between NT_{1-154} and GST-pCT/CaM compared to Ca^{2+}-free conditions (**Fig. 4Cd**), as seen previously (**Figures 2 and 3**). Strikingly, all pNT mutations except NT_{1154}RPPR eliminate the Ca^{2+}-sensitivity of NT-pCT binding; the mutated NT_{1-154} binds pCT/CaM similarly both in the absence of Ca^{2+} and in high Ca^{2+} (compare blue and dark red bars in **Fig. 4Cd**). Importantly, these are the same mutations that, by themselves, reduce the NT-pCT binding in the absence of Ca^{2+} (NT_{1-154}ALL, NT_{1-154}PIRR, NT_{1-154}ACI and NT_{1-154}SIV). In other words, many mutations along the pNT appear to mimic the effect of high-Ca^{2+} on NT-pCT/CaM binding. A parsimonious interpretation for all the data of **Fig. 4C** is that the pNT not only participates in the pCT binding, but also takes part in Ca^{2+}-induced reduction in NT-pCT/CaM interaction.

Functional effects of mutations that alter NT-CT interaction

Given the importance of the pNT for the Ca^{2+}-induced changes in NT-pCT interaction, as revealed in the experiments of **Figure 4C**, we tested the effects of the pNT mutations on channel function. We introduced the same NT mutations into the intact channel and tested activation (current-voltage relation, I-V, and conductance-voltage relation, G-V) and inactivation (kinetics) properties of the Ca^{2+} and Ba^{2+} currents (I_{Ca} and I_{Ba}, respectively) of mutated α_{1C} in *Xenopus* oocytes (**Fig. 5**). None of the mutations significantly affected the I-V and G-V relations (**Fig. 5B**, second column, and data not shown).

Both I_{Ba} and I_{Ca} inactivate during depolarization [37] (see **Figure 5B**, 1st column from the left). Kinetics of inactivation were routinely characterized using the r_{400} parameter, calculated as the ratio [current 400 ms after the beginning of the depolarizing pulse]/[peak current amplitude]. [29,30] Low r_{400} reports strong inactivation; r_{400}=1 when there is no inactivation. The dependence of r_{400} on V_m of all the mutated channels has the typical U-shaped form in I_{Ca} which disappears in I_{Ba} (**Fig. 5B**, 3rd column). r_{400} of the mutated channels at 20 mV (**Fig. 5B**, 4th column) indicates that the mutated channels α_{1C}CLT and α_{1C}PIR/R have significantly stronger I_{Ba} and I_{Ca} inactivation (changes in I_{Ba} were more robust) compared to the control channel (WT channel). The stronger inactivation suggests that replacing these a.a. with alanine removes some kind of obstacle that normally slows the inactivation. Overall, all the pNT mutations either accelerated the inactivation or did not change it, implying that the NT plays a general role in suppression of inactivation. f_{400}, the difference between r_{400} of I_{Ba} and I_{Ca} which indicates the Ca^{2+} component of inactivation, [10,37] was reduced in CLT and PIR/R and also in ALL and SIV mutants (**Fig. 5B**, note the f_{400} values on the right). Thus, mutations CLT, PIR/R, ALL and SIV reduce the Ca^{2+}-dependent component of total inactivation.

In summary, the binding experiments showed that several mutations weaken the NT-pCT interaction under Ca^{2+}-free conditions, and some mutations strengthen the interaction in the presence of Ca^{2+}. We compared the changes in binding to altered inactivation of I_{Ca} and I_{Ba}. This comparison indicates 3 trends caused by the majority of mutations: (i) reduction in NT-pCT binding under Ca^{2+}-free conditions, (ii) an acceleration of I_{Ba} inactivation, and (iii) a reduction in f_{400}, which corresponds to a reduction in Ca^{2+}-induced acceleration of inactivation.

Further comparison of I_{Ba} inactivation of the mutated channels to the control channel at different time points reveals that the pNT mutations generally have only a small effect on the fast component of I_{Ba} inactivation (after 400 ms, **Fig. 5** and **Fig. 6A**), and a stronger effect on the slow component (after 2000 ms or 10000 ms, **Fig. 6B and C**, respectively) of I_{Ba} inactivation. Generally, all mutations in pNT (especially CLT and PIR/PIRR) accelerated the inactivation of I_{Ba}, suggesting that this region is important for a slow component of voltage-dependent inactivation (whose nature is not known).

Discussion

NT-CT interaction and its dependence on Ca^{2+}

Interaction between NT and CT of a channel is neither a new idea nor exclusive for Ca^{2+} channels. For example, the 4

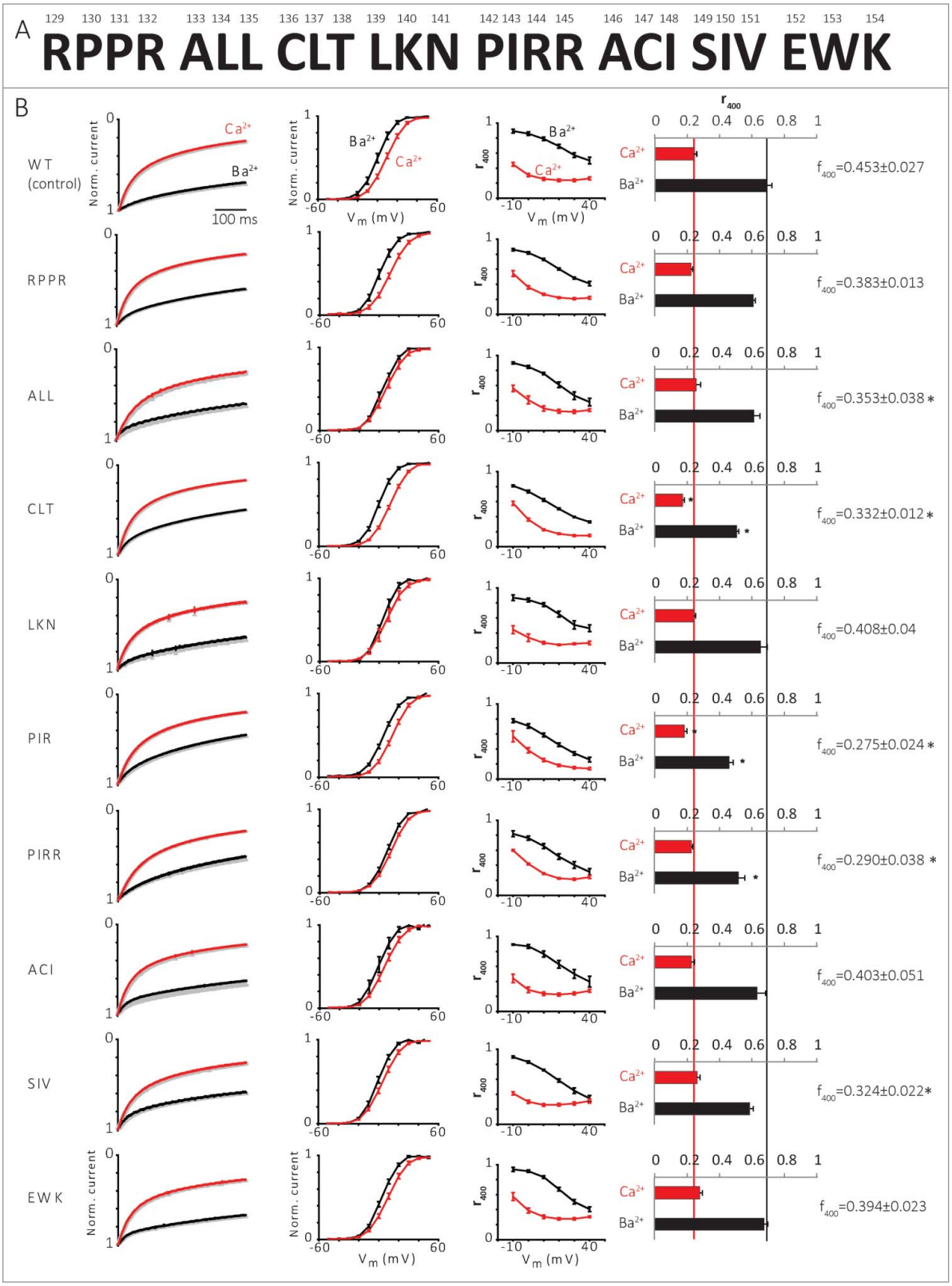

Figure 5. Effect of NT mutations on I_{Ca} and I_{Ba}. (**A**) 129-154 NT a.a. arranged in triples or quadruples which were mutated to alanines. (**B**) Inactivation of the channel with Ba^{2+} and Ca^{2+}. From left to right: 1st column, normalized averaged I_{Ba} (black) and I_{Ca} (red) currents (3-15 oocytes in each group) measured at +20 mV. 2nd column, voltage-conductance (G-V) curve. 3rd column, fraction of peak current after 400 ms depolarization (r_{400}) of I_{Ba} and I_{Ca} at different voltages. 4th column, fraction of peak current after 400 ms depolarization (r_{400}) of I_{Ba} and I_{Ca} at 20 mV, *$P < 0.05$. 5th column, the difference between r_{400} of I_{Ba} and I_{Ca} (f_{400}), *$P < 0.05$.

subunits of the K^+ channels $KCNQ_2$ and $KCNQ_3$ have an NT-CT interaction[38] and in the rat olfactory CNG channel, the interaction of NT with CT promotes channel activation.[39] The involvement of CaM in the NT-CT interaction also appears in other channels, such as CNG, where CaM binding to the NT disrupts the NT-CT interaction, leading to channel inactivation.[39,40] However, Ca^{2+} channels, unlike CNG or K^+ channels composed of 4 separate subunits (each with an NT and a CT), have only one NT and CT. The idea of an interaction between NT and CT in α_{1C}, and for a role of this interaction (within a hypothetical "NT-CT scaffold")[10] in channel gating and inactivation, has been already raised in the past.[4,10] However, our current work shows that the details of this interaction and its function are different from the previously envisioned ones.

In this study we demonstrate, for the first time, that there is a direct physical interaction between the NT and pCT of $Ca_V1.2$ α_{1C} subunit. Furthermore, we show the formation of a ternary complex of NT-pCT-CaM *in vitro*. Importantly, the NT-pCT/CaM interaction is reduced in the presence of high Ca^{2+}. Quantitative experiments using microscale thermophoresis (MST) indicate an approximately 4-fold reduction in interaction affinity when going from nominally Ca^{2+}-free conditions to 12-100 μM (**Fig. 3**), which corresponds to physiological Ca^{2+} levels attained in the Ca^{2+}-CT interaction nanodomain upon Ca^{2+} entry that follows channel's opening.[2] Ca^{2+}-induced reduction in NT-pCT binding was confirmed in pull-down experiments using different protocols and with purified as well as *in vitro* synthesized NT and pCT segments.

We were able to assess the affinity of NT-pCT-CaM interaction in the presence of 0.1-1 mM Ca^{2+} using 2 different purified recombinant pCT constructs, where CaM was either present as a separate but co-purified protein, or it was fused to the pCT via a peptide linker. The apparently higher affinity observed with the non-fused pCT/CaM (0.3 μM) vs. the fused pCT-lnk-CaM (3-4 μM) could be due to the difference in the protein construct itself or in the method used (FP vs. MST, respectively). Whatever the reason for this difference, it is evident that the binding affinity of NT-CT/CaM interaction in solution is in the sub-micromolar or low-micromolar range. The affinity of interaction in Ca^{2+}-free conditions, as estimated by MST, is sub-micromolar (**Fig. 3**). Since NT and CT are parts of the same protein in the native channel, the relative effective concentration of these channel termini is very high, thus a robust interaction is predicted between these regions in the intact $Ca_V1.2$.

Mapping of the NT-pCT interaction determinants within the NT by deletion and single a.a. mutants points to a complex binding surface comprising the initial (distal) and proximal (close to plasma membrane, pNT) parts of the NT, and possibly additional segments. Furthermore, mutagenesis of the last 25 a.a. of the NT suggests that pNT contributes to the NT-pCT interaction particularly in low Ca^{2+}. Structural elucidation of the NT and pCT interface and the Ca^{2+}-induced changes are an important challenge for the future.

NT-CT interaction may be involved in Ca^{2+}-induced inactivation process

In this study, we have begun the exploration of the importance of the NT-CT interaction for the regulation of the channel. At this stage, we explored the functional consequences of mutations within the pNT, a segment which appears to play an important role in Ca^{2+}-induced changes in NT-pCT interaction. Our results suggest that the NT-CT interaction does not alter the voltage-dependent activation of $Ca_V1.2$ but it regulates the channel's inactivation. We compared I_{Ba} inactivation (generally considered to represent the voltage-dependent inactivation) and the faster I_{Ca} inactivation. The latter occurs when both depolarization and Ca^{2+} entry take place and is usually viewed as an acceleration, by Ca^{2+}, of the voltage-dependent process, although it is not known whether and how the 2 processes are coupled.[41,42] Several pNT mutations, in particular $LL_{134-135}$, $CLT_{136-138}$ and $PIRR_{142-145}$ to alanines, accelerated I_{Ba} inactivation, whereas the inactivation of I_{Ca} was only slightly affected (**Figs. 5, 6**). Notably, the same mutations both reduced the NT-pCT interaction in the absence of Ca^{2+}, and eliminated the Ca^{2+}-induced reduction in NT-pCT binding (**Fig. 4**). All mutations that weakened NT-CT binding in the absence of Ca^{2+} reduced the net effect of Ca^{2+} on inactivation kinetics, as indicated by the reduction in f_{400} parameter (**Fig. 5**). Thus, mutations that mimicked the effect of Ca^{2+} on NT-pCT binding, also partially recapitulated the accelerating effect of Ca^{2+} on inactivation. These findings indicate coupling between Ca^{2+}-induced changes in NT-CT interaction and acceleration of inactivation by Ca^{2+} entry in the $Ca_V1.2$ channel.

We propose a model in which Ca^{2+} entry may induce a weakening of the NT-CT interaction, and the ensuing rearrangement of the cytosolic domain is allosterically transmitted to the channel's gate(s) to accelerate inactivation. Accordingly, perturbations (such as mutations) that weaken the NT-CT interaction accelerate inactivation already in the absence of Ca^{2+} and, consequently, diminish the relative accelerating effect of Ca^{2+}. This mechanism may account for all of the Ca^{2+}-induced acceleration of inactivation, or be a part of a more complex mechanism where additional Ca^{2+}/CaM-induced processes take place.

Ca^{2+} entry may cause a rearrangement of the cytosolic area of the channel

The domain-swapped architecture of the transmembrane domain of voltage-dependent channels places the pore (S5-S6) from domain IV, which is connected to pCT, next to the voltage sensor (S1-S4) from domain I (connected to NT) and ensures cooperativity between these 2 domains and the 2 termini.[43] Binding experiments *in vitro* indicate a weaker NT-pCT interaction under high-Ca^{2+} vs. Ca^{2+}-free (EGTA) conditions. The interaction between the NT and the pCT in Ca^{2+} buffer still persists, albeit with a reduced affinity, perhaps in a different configuration. Most of the pNT mutations that we introduced reduced NT-CT binding under Ca^{2+}-free conditions, and weakened the Ca^{2+}-induced reduction of NT-CT binding. This finding implies that it will be easier to

produce the hypothesized NT-CT rearrangement in the mutated channels, making it easier for the mutants to reach the inactivated state, resulting in the observed acceleration in I_{Ba} inactivation seen in most mutants. Thus, according to our model, the more avid NT-pCT interaction under Ca^{2+}-free conditions may also explain the difference between I_{Ca} inactivation vs. I_{Ba} inactivation. When Ba^{2+} is the carrier ion and [Ca^{2+}] remains at its resting low level, the NT-pCT domains are bound tightly and consequently the I_{Ba} inactivation is slower than the I_{Ca} inactivation.

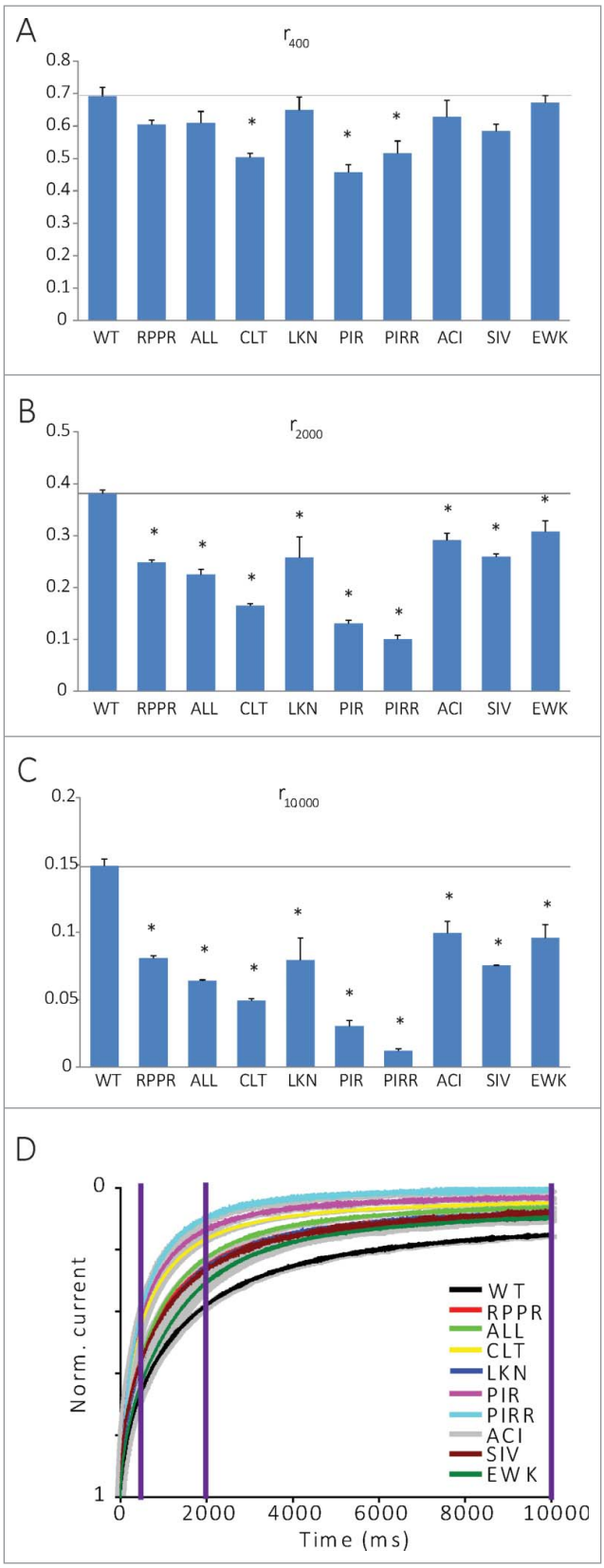

The role of CaM

Our results argue against the formation of an NT-CT bridge by CaM, previously proposed as a part of the mechanism of Ca^{2+}-CaM-dependent inactivation.[4,10] Pull-down experiments show that NT_{60-99} (which includes the NSCaTE area) binds CaM but does not bind the pCT. We also saw no interaction between NT_{60-120} and pCT under Ca^{2+}-free conditions or in the presence of Ca^{2+}-CaM [35] (**Fig. 4**). In contrast, the NT_{1-154} WIR mutant in which the mutated NSCaTE domain cannot bind CaM, does form such a ternary NT-pCT-CaM complex. The lack of evidence for the formation of a ternary NT_{60-120}-pCT-CaM complex, even in pull down experiments where all 3 proteins are present at over-expression levels, suggests that the NT-pCT interaction occurs directly through a region outside the NSCaTE.

Nevertheless, since CaM is the uncontested Ca^{2+} sensor for Ca^{2+}-induced inactivation,[8] the first event in this process must be the binding of Ca^{2+} to CaM, already docked at pCT as apo-CaM, followed by structural rearrangements at the pCT.[44] We propose that this change is followed by a rearrangement of the NT-pCT-CaM scaffold. Our *in vitro* experiments do support a major role for CaM in mediating the Ca^{2+}-induced rearrangement of the NT-CT scaffold, because CaM was essential for the Ca^{2+}-induced reduction in NT-CT binding at physiologically relevant Ca^{2+} levels (**Fig. 2**).

It is not clear whether and how the NT's CaM-binding segment NSCaTE is involved in the mechanism described here. Binding of CaM (the same one anchored at the CT, or a separate additional CaM molecule) to the NT, in the presence of elevated Ca^{2+} concentration, could contribute to the weakening of CaM-independent NT-CT interaction. The possibility that an additional CaM binds to the ternary NT-CT-CaM complex in the presence of Ca^{2+} is theoretically plausible, because the VGCC acts as a 'magnet' for CaM molecules and is locally enriched with CaM in the channel's nanodomain, up to an estimated 2.5 mM.[45] This second CaM can interact with NSCaTE. The affinity of the NScaTE to Ca^{2+}-CaM is below 1 μM. [35] Although this is ~1000 times lower compared to the IQ domain,[46] after channel opening there is enough Ca^{2+}-CaM to saturate the NSCaTE.

Proposed molecular mechanism of $Ca_V1.2$ modulation through NT-pCT interaction

We propose a molecular mechanism based on findings from this work and other published studies (**Fig. 7**). Under conditions

Figure 6. NT mutations have little effect on the fast component of I_{Ba} inactivation and a stronger effect on the slow component. (**A**) Fraction of peak current after 400 ms depolarization (r_{400}) of I_{Ba}. *P < 0.05. (**B**) Fraction of peak current after 2000 ms depolarization (r_{2000}) of I_{Ba}. *P < 0.05. (**C**) Fraction of peak current after 10000 ms depolarization (r_{10000}) of I_{Ba}, N is between 3 and 10 cells. *P < 0.05. (**D**) Normalized averaged I_{Ba} currents over 10000 ms.

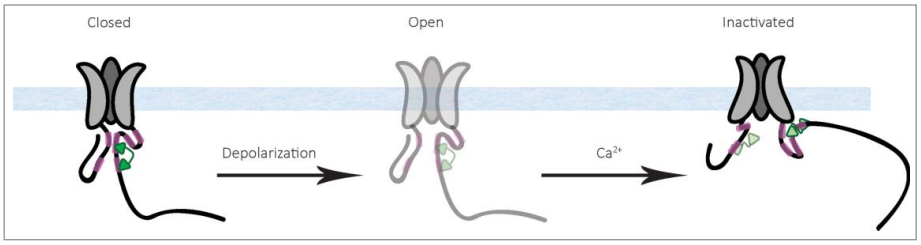

Figure 7. Proposed molecular mechanism of $Ca_V1.2$ modulation. CaM is bound to the CT at preIQ and IQ sites, the NT and CT of the channel are interacting, the channel is closed (left). The channel opens (middle), Ca^{2+} enters, binds to CaM, the NT and CT rearrange and the channel is inactivated (right). In the inactivated conformation, the possibility that a second CaM (light green) becomes bound to the NSCaTE is indicated.

of low Ca^{2+} levels, apoCaM interacts with the IQ and preIQ domains of the closed channel. While $CaM_{C\text{-}lobe}$ interacts with IQ, $CaM_{N\text{-}lobe}$ interacts with preIQ.[47] We cannot rule out the possibility of $CaM_{N\text{-}lobe}$ not interacting with the pCT at all, as in the Na_V channels.[48] We demonstrated an interaction between NT and pCT/CaM; Ca^{2+} reduces the affinity of this interaction. Depolarization opens the channel, Ca^{2+} enters through the pore raising the Ca^{2+} levels in the nano-domain of the channel. The CaM bound to the pCT, now with 4 Ca^{2+} (Ca^{2+}-CaM), changes its conformation and embraces the IQ with both lobes,[49] driving rearrangements within NT-CT scaffold (presented in **Figure 7**, for illustration purposes, as distancing of NT from the CT). This rearrangement promotes inactivation. How this happens is not yet known, but we further propose that the NT and CT channel domains serve as levers whose movements promote changes in the transmembrane core of the channel (narrowing or broadening it) via S1 (NT) or S6 (pCT), akin to our observations regarding the I-II linker [28] and not as a kind of physical gate blocker. CaM can promote or restrain these movements and thus influence the inactivation of the channel. Mutations in these cytoplasmic areas can change the inactivation either by weakening/strengthening the interaction between distinct cytoplasmic areas, or by disrupting the structural elements involved in the transfer of the movements of the cytoplasmic parts to the pore/gate.

Experimental Procedures

Molecular biology

DNA constructs

cDNA constructs of rabbit heart α_{1C} (X15539), β_{2b} (L06110), $\alpha_2\delta_1$ (P13806), CaM, CaBP1 and the segments (NT and pCT) are in the pGEM vector which contains 5′ and 3′ untranslated regions (UTRs) from *Xenopus* β-globin. GST protein constructs are in the pGEX-4 vector. New cDNA constructs were obtained using standard PCR procedures and fully sequenced.

RNA preparation

RNA was prepared by *in vitro* transcription from linearized DNA (6.5μg), at 37°C. T7 polymerase was used for the preparation of pGEM constructs RNA. The RNAs were kept separately at −80°C and mixed before the injection for the expression of many proteins.

Heterologous expression system in Xenopus oocytes

Maintenance of frogs (*Xenopus laevis*) and preparation of oocytes was as described.[50] Experiments were approved by Tel Aviv University Institutional Animal Care and Use Committee (permits M-08-081 and M-13-002). mRNA (0.5-5 ng/oocyte) of each subunit was injected into the oocyte which was incubated at 20-22°C in NDE solution (96 mM NaCl, 2 mM KCl, 1 mM $MgCl_2$, 1 mM $CaCl_2$, 5 mM HEPES, PH=7.5) for 3-5 days before measuring currents. In case of Ca^{2+} currents or massive Cl^- currents, the oocytes were injected with 25-50 nl of the Ca^{2+} chelator BAPTA about 15 min prior to the measurement. The BAPTA effect lasts about 2 hours after the injection.

Electrophysiology

Two-electrode voltage clamp (TEVC) techniques were used to measure Ba^{2+} or Ca^{2+} currents in *Xenopus* oocytes, using inactivation and IV protocols. Ba^{2+} currents were measured in a high Ba^{2+} solution (40mM $Ba(OH)_2$, 5mM HEPES, 50mM NaOH, 2mM KOH, pH=7.5) and Ca^{2+} currents were measured with a high Ca^{2+} solution (40mM $Ca(OH)_2$, 5mM HEPES, 50mM NaOH, 2mM KOH, pH=7.5), which were titrated to pH 7.5 with methanesulfonic acid. Each protocol was measured with a high Ba^{2+}/Ca^{2+} solution with or without addition of 200 μM Cd^{2+} (Ca^{2+} channel blocker, which allows measurement of non-Ca^{2+} channels currents in the oocyte). The net current was obtained by subtracting the Cd^{2+} current from the one without Cd^{2+}. Data analysis was performed using the pCLAMP software (Axon Instruments). Graphs and statistical analysis were performed with SigmaPlot (SPSS, Inc.., Chicago, IL).

The current–voltage (I-V) curve was fitted to the Boltzmann equation:

$$I_{Ba} = G_{max}(V_m - V_{rev}) / (1 + \exp(-V_m - V_{1/2}) / K_a)$$

where K_a is the slope factor, $V_{1/2}$ is the voltage that causes half maximal activation, G_{max} is the maximal macroscopic conductance, V_m is membrane voltage, I_{Ba} is the current measured at the same voltage, and V_{rev} is the reversal potential of I_{Ba}. The obtained parameters of G_{max} and V_{rev} were then used to calculate fractional conductance at each V_m, G/G_{max}, using the equation:

$$G / G_{max} = I_{Ba} / (G_{max}(V_m - V_{rev}))$$

Where G is the total macroscopic conductance at V_m. The conductance–voltage (G-V) curves were plotted with the values of $V_{1/2}$ and K_a obtained from the fit of the I-V curves, using the

following form of the Boltzmann equation:

$$G / G_{max} = 1/ (1 + \exp(-(V_m - V_{1/2})/K_a))$$

Protein preparation

GST-fused proteins

The GST-fused proteins were expressed in *Escherichia coli* BL21 cells. Cultures were grown in a shaker device, in a 2xYT medium (16g/L Trypton, 10g/L Yeast extract, 5g/L NaCl), induced at OD 0.4-0.6 with 0.1 mM IPTG, and followed by further 37°C incubation for 3 h. The cells were separated from the medium by centrifugation at 7000 RPM for 10 minutes at 4°C and preserved for at least one night at −80°C. After thawing, the cells were suspended in Phosphate Buffered Saline (PBS), 1 mM PMSF and 1 mM DNAse, and disrupted using a homogenizer, followed by a micro-fluidizer (Microfluidics, Newton, MA). Next, we separated the proteins from the non-soluble precipitates of the cell by centrifugation at 12000 RPM for 40 minutes at 4°C. All the proteins were produced from the cell's soup. The proteins were purified on ÄKTAprime (GE Healthcare, USA) with GST-affinity chromatography, followed by gel-filtration chromatography in the experiment buffer. The protein concentrations were determined by Bradford at $\lambda = 595$ nm or by absorbance at $\lambda = 280$ nm.

$pCT_{1508-1669}$/CaM and $pCT_{1508-1669}$ (C1564S)/CaM

E. coli pellet was resuspended in 50 mM sodium phosphate pH 8.0, 0.35 M NaCl, 20% glycerol, DNase (15 units/ml), lysozyme and 1 mM PMSF. Clarified lysate was loaded onto a Ni^{2+} chelate column (Ni^{2+}CaM, Sigma), pre-equilibrated with buffer A. The column was extensively washed to remove non-specifically bound contaminating proteins prior to elution by a linear gradient of imidazole (5-150 mM). Eluted fractions were immediately collected, concentrated and loaded onto a HiLoad 16/60 Superdex 200 gel filtration column (GE Healthcare), pre-equilibrated with GF1 buffer (20 mM Tris pH 7.5, 0.5 M NaCl, 5 mM Imidazole, 25 % glycerol, 10 μM CaCl2). Collected fractions were subjected to overnight TEV proteolysis at 4°C. Proteins were then run again through a Ni^{2+} chelate column pre-equilibrated with GF1 buffer. Concentrated column flow through was then loaded onto a Superdex-200 gel filtration column pre-equilibrated with GF2 buffer (20 mM Tris-HCl pH 7.5, 125 mM NaCl, 5 mM 2-mercaptoethanol). Selected fractions were then collected, concentrated and stored at −80°C. For the $pCT_{1508-1669}$ (C1564S)/CaM complex, the protein was subjected to fluorescein labeling prior to loading onto the gel filtration column. For FP measurements, proteins were labeled via thiol modifications at cysteine residues using the reactive dye fluorescein-5-maleimide (Anaspec). Fluorescent dye was freshly dissolved in DMSO and mixed at 1:100 dye:protein ratio with the protein solution (100 μM). Following a 2 hour incubation at dark in room temperature, the reaction was stopped by the addition of 1 mM glutathione. Separation of protein from excess dye was then attained by gel filtration/desalting as described for each protein.

$pCT_{1508-1669}$(C1564S)-lnk-CaM

Rabbit $\alpha_{1C\ 1508-1669}$ was fused with calmodulin by a peptide linker (AAADLEVLFQGPLH). The upstream of proximal C terminus has MGSHHHHHHHHGSDYDIPTTENLYFQGS. E. coli pellet was suspended at a ratio of 10 ml buffer per 1 gm pellet in lysis buffer (20 mM Tris-HCl buffer pH-7.5, 0.5 M NaCl, 20% glycerol, 10 mM 2-mercaptoethanol, DNase (15 units/ml), lysozyme, 0.1 % TritonX and 1 mM PMSF). The lysate was homogenized and cells were lysed by ultrasonication. Cell debris were removed by centrifugation for 50 min at 15000 rpm at 4° C. Subsequently, supernatant was loaded on a Ni^{2+}-NTA (Qiagen) column, pre-equilibrated with buffer A (20 mM Tris-HCl buffer pH-7.5, 0.5 M NaCl, 20% glycerol, 10 mM 2-mercaptoethanol) at a flow rate of 1ml/min. The column was extensively washed by buffer A, containing 9 mM imidazole to remove non-specifically bound contaminating proteins prior to elution by buffer A containing 150 mM imidazole. Elution profiles were monitored at 280 nm. Eluted fractions were immediately collected, concentrated and loaded onto a Superdex 200 gel filtration column (GE Healthcare), pre-equilibrated with GF1 buffer. Selected fractions were collected, concentrated and stored at −80° C. These fractions were further used for dye labeling via thiol modification at cysteine residues using the reactive NT-647-Maleimide fluorescent dye (Nano Temper Technologies). The buffer exchange of the protein was done using the provided buffer and spin column following the procedures mentioned by the manufacturer. Fluorescent dye was freshly dissolved in DMSO and mixed at 10:1 dye:protein ratio with the protein solution (10 μM) following one hour incubation at dark in room temperature. The unreacted dyes were separated from the protein using the gravity flow column using the buffer 20 mM Tris-HCl pH-7.5, 200 mM NaCl, 25% glycerol, 1 mM DTT. The labeled proteins were flash-frozen in liquid nitrogen in several aliquots and stored at −80° C and subsequently used for microscale thermophoresis experiments.

MBP-NT fusion proteins

MBP-NT_{60-120}, MBP-NT_{1-134} and MBP-NT_{1-154} were co-expressed with CaM while MBP-$NT_{135-154}$ and MBP-$NT_{100-154}$ were expressed alone. Cells were resuspended in Ni^{2+} column buffer (50 mM Tris-HCl pH 7.5, 0.3 M NaCl, 20% glycerol, 5 mM CaCl2 (only for MBP-NT/CaM)). Ni^{2+} chelate column eluted protein was then diluted by the addition an equivalent volume of: 20 mM Tris-HCl pH 7.5, 0.3 M NaCl, 20% glycerol, 20 mM 2-mercaptoethanol, 2 mM EDTA. For the MBP-NTx/CaM proteins, dilution solution also contained 10 mM EGTA in order to assure the separation of the complex. Diluted protein was loaded onto an amylose resin (NEB) column pre-equilibrated with: 20 mM Tris-HCl pH 7.5, 0.3 M NaCl, 20% glycerol, 10 mM 2-mercaptoethanol, 1 mM EDTA. Isolated MBP-NTx proteins were eluted by the addition of 10 mM maltose. Further purification was performed using Superdex 200 gel filtration in: 20 mM Tris-HCl pH 7.5, 200 mM NaCl, 1 mM DTT.

MST analysis

Binding experiments were carried out with Monolith NT.115 (Nano Temper Technologies GMBH, München, Germany). Ten microliters of 100 nM NT-647 labeled $pCT_{1508-1669}$(C1564S)-linker-CaM were mixed with 10 μl of various concentrations of MBP-NT_{1-154} (2 nM to 20 μM) and mixed in PCR tubes. Subsequently, the samples were loaded on standard treated capillaries. All the binding experiments were carried out at 25° C, using 60% LED power with 80% MST power. Experiments were carried out in 20 mM Tris-HCl buffer pH-7.5, 200 mM NaCl, 1 mM DTT, 25% glycerol, 0.05% Tween 20. The concentration of Ca^{2+} was varied from 1 to 0 mM and the concentrations of Ca^{2+} were maintained using EDTA with $CaCl_2$ solutions. Data analysis was performed with the Monolith software using the thermophoresis and T-jump process.

Fluorescence polarization measurements

Increasing concentrations of unlabeled target protein were mixed with nM concentrations of fluorescein tagged "bait" proteins and incubated on ice in the dark for 5 minutes. Steady-state fluorescence polarization measurements were then taken using either an ISS K2 or a Horiba Jobin-Yvon FluoroLog-3 spectrofluorometer at 10° C using excitation and emission wavelengths of 492 and 522 nm, respectively. Five to 10 repeated polarization measurements were taken for each sample with integration times and instrumental parameters yielding a maximum standard deviation of 5% between repeats. Triplicates were taken for each data point in most cases although in some cases, a duplicate was taken due to lack of material. Polarization data was analyzed using Sigmaplot (Systat Software, Inc.). Polarization change from baseline (ΔP) to target protein concentration relations were fitted by nonlinear regression (ligand binding macro) to a one site saturation model by the following equation: $\Delta P = NX + B_{max} \times X / (K_D + X)$, where X is the concentration of free target protein (ligand); B_{max}, the maximum change in polarization upon saturation; K_D, the concentration of ligand required to reach half-maximal binding; N, non-specific binding between the bait and target proteins.

Pull down with S^{35}-Met labeled proteins experiments

Different parts of the $Ca_V1.2$ channel were translated *in vitro* from the appropriate RNA using rabbit reticulocyte lysate, according to standard protocols. The S^{35}-Met labeled lysate and GST-fused proteins were incubated in high Ca^{2+}/Ca^{2+}-free (EGTA) binding buffer (150 mM KCl, 50 mM Tris, 5 mM $MgCl_2$, 1 mM $CaCl_2$/EGTA, pH=7.0) with 0.5% CHAPS (3-[(3-cholamidopropyl) dimethylammonio] - 1-propanesulfonic acid). After incubation for 30 minutes at 30°C, the total volume was completed to 300 μl with the same buffer and incubated for another 30 minutes. Next, a sample of the input (5 μl of the 300 μl inserted into the reaction, 1/60) was removed, to be loaded later on the gel as "input," and 30 μl glutathione-Sepharose beads (Amersham Pharmacia Biotech) were added. The reaction was incubated again for 30 minutes at 4°C, with rotation, and then washed 3 times from non-specific binding with the same buffer. The GST-fused proteins and any associated molecules were eluted with excess free glutathione in the elution buffer (120 mM NaCl, 100 mM Tris-HCl, pH 8, 30 μl). The proteins were resolved on a 12% SDS polyacrylamide gel, stained with 12.5% Coomassie brilliant blue R-250 (Bio-rad) and processed for further analysis by autoradiography for at least 3 days exposure before the identification of the labeled products with Phosphor-imager (Molecular dynamics).

Pull-down with MBP proteins experiments

In order to co-express the HisTagged $pCT_{1508-1669}$, CaM and an MBP (and His) tagged fragment of the $Ca_V1.2$ NT (MBP-NTx), E.coli cells were transformed with a mixture of either the pET-Duet $pCT_{1508-1669}$/CaM vector and pET28 MBP-NTx or pET-Duet $pCT_{1508-1669}$ with CDF MBP-NTx/CaM expression vectors. Cell growth and protein expression induction were similar to the described above. Harvested E. coli pellet was resuspended in binding buffer (50 mM Tris-HCl pH 7.5, 0.2 M NaCl, 5 mM $CaCl_2$, 20% glycerol). Cell lysis was then performed by sonication and was followed by a 30 min centrifugation at 14000 rpm, 4°C. The soluble fraction (1 ml) was then removed and incubated with 40 μl of buffer equilibrated Ni^{2+} chelate beads at 4°C for 1-2 h. Subsequently, beads were pelleted and washed with binding buffer prior to protein elution by 500 μl of binding buffer added with 250 mM imidazole. Eluted protein was then incubated again with 40 μl of buffer equilibrated amylose resin at 4°C for 1-2 h. Subsequent to incubation, beads were washed for 3 times with binding buffer to remove unbound proteins. A sample from the last wash was collected to analyze for traces of the unbound proteins as a control. Proteins were then eluted with 30 μl of binding buffer plus 10 mM maltose and analyzed by Tricine–SDS–PAGE.

Statistics and Data Presentation

Comparison between several groups was performed using one-way analysis of variance (ANOVA) followed by Dunnet's test, using the SigmaPlot software (SPSS Corp.). Data presentation was carried out using Excel (Microsoft) and SigmaPlot (SPSS Corp.).

Disclosure of Potential Conflicts of Interest

No potential conflicts of interest were disclosed.

Funding

This work was supported by the German-Israeli Foundation for Scientific Research and Development, grant # I-1210-286.13/2012, the Fields Funds for Cardiovascular Research to ND, and by DIP (DFG) and Israel Science Foundation (1519/12) grants to JAH.

References

1. Clapham DE. Calcium signaling. Cell 2007; 131:1047-58; PMID:18083096; http://dx.doi.org/10.1016/j.cell.2007.11.028
2. Tadross MR, Dick IE, Yue DT. Mechanism of local and global Ca^{2+} sensing by calmodulin in complex with a Ca^{2+} channel. Cell 2008; 133:1228-40; PMID:18585356; http://dx.doi.org/10.1016/j.cell.2008.05.025
3. Catterall WA. Structure and regulation of voltage-gated Ca^{2+} channels. Annu Rev Cell Dev Biol 2000; 16:521-55; PMID:11031246; http://dx.doi.org/10.1146/annurev.cellbio.16.1.521
4. Dick IE, Tadross MR, Liang H, Tay LH, Yang W, Yue DT. A modular switch for spatial Ca^{2+} selectivity in the calmodulin regulation of Ca_v channels. Nature 2008; 451:830-4; PMID:18235447; http://dx.doi.org/10.1038/nature06529
5. de Leon M, Wang Y, Jones L, Perez-Reyes E, Wei X, Soong TW, Snutch TP, Yue DT. Essential Ca^{2+}-binding motif for Ca^{2+}-sensitive inactivation of L-type Ca^{2+} channels. Science 1995; 270:1502-6; PMID:7491499; http://dx.doi.org/10.1126/science.270.5241.1502
6. Zhou J, Olcese R, Qin N, Noceti F, Birnbaumer L, Stefani E. Feedback inhibition of Ca^{2+} channels by Ca^{2+} depends on a short sequence of the C terminus that does not include the Ca^{2+}-binding function of a motif with similarity to Ca^{2+}-binding domains. Proc Natl Acad Sci U S A 1997; 94:2301-5; PMID:9122189; http://dx.doi.org/10.1073/pnas.94.6.2301
7. Kim EY, Rumpf CH, Van Petegem F, Arant RJ, Findeisen F, Cooley ES, Isacoff EY, Minor DL Jr. Multiple C-terminal tail Ca^{2+}/CaMs regulate $Ca_V1.2$ function but do not mediate channel dimerization. EMBO J 2010; 29:3924-38; PMID:20953164; http://dx.doi.org/10.1038/emboj.2010.260
8. Ben-Johny M, Yue DT. Calmodulin regulation (calmodulation) of voltage-gated calcium channels. J Gen Physiol 2014; 143:679-92; PMID:24863929; http://dx.doi.org/10.1085/jgp.201311153
9. Kanevsky N, Dascal N. Regulation of maximal open probability is a separable function of Ca_Vb subunit in L-type Ca^{2+} channel, dependent on NH2 terminus of a_{1C} ($Ca_V1.2a$). J Gen Physiol 2006; 128:15-36; PMID:16801381; http://dx.doi.org/10.1085/jgp.200609485
10. Ivanina T, Blumenstein Y, Shistik E, Barzilai R, Dascal N. Modulation of L-type Ca^{2+} channels by Gbg and calmodulin via interactions with N- and C-termini of a_{1C}. J Biol Chem 2000; 275:39846-54; PMID:10995757; http://dx.doi.org/10.1074/jbc.M005881200
11. Zhou H, Yu K, McCoy KL, Lee A. Molecular mechanism for divergent regulation of $Ca_V1.2$ Ca^{2+} channels by calmodulin and Ca^{2+}-binding protein-1. J Biol Chem 2005; 280:29612-9; PMID:15980432; http://dx.doi.org/10.1074/jbc.M504167200
12. Kobrinsky E, Schwartz E, Abernethy DR, Soldatov NM. Voltage-gated mobility of the Ca^{2+} channel cytoplasmic tails and its regulatory role. J Biol Chem 2003; 278:5021-8; PMID:12473653; http://dx.doi.org/10.1074/jbc.M211254200
13. Chou JJ, Li S, Klee CB, Bax A. Solution structure of Ca^{2+}-calmodulin reveals flexible hand-like properties of its domains. Nat Struct Biol 2001; 8:990-7; PMID:11685248; http://dx.doi.org/10.1038/nsb1101-990
14. Halling DB, Aracena-Parks P, Hamilton SL. Regulation of voltage-gated Ca^{2+} channels by calmodulin. Sci STKE 2006; 2006:er1; PMID:16685765
15. Chin D, Means AR. Calmodulin: a prototypical calcium sensor. Trends Cell Biol 2000; 10:322-8; PMID:10884684; http://dx.doi.org/10.1016/S0962-8924(00)01800-6
16. Mruk K, Shandilya SM, Blaustein RO, Schiffer CA, Kobertz WR. Structural insights into neuronal K^+ channel-calmodulin complexes. Proc Natl Acad Sci U S A 2012; 109:13579-83; PMID:22869708; http://dx.doi.org/10.1073/pnas.1207606109
17. Biswas S, DiSilvestre DA, Dong P, Tomaselli GF. Mechanisms of a human skeletal myotonia produced by mutation in the C-terminus of $Na_V1.4$: is Ca^{2+} regulation defective? PLoS One 2013; 8:e81063; PMID:24324661; http://dx.doi.org/10.1371/journal.pone.0081063
18. Ben-Johny M, Yang PS, Niu J, Yang W, Joshi-Mukherjee R, Yue DT. Conservation of Ca^{2+}/calmodulin regulation across Na and Ca^{2+} channels. Cell 2014; 157:1657-70; PMID:24949975; http://dx.doi.org/10.1016/j.cell.2014.04.035
19. DeMaria CD, Soong TW, Alseikhan BA, Alvania RS, Yue DT. Calmodulin bifurcates the local Ca^{2+} signal that modulates P/Q-type Ca^{2+} channels. Nature 2001; 411:484-9; PMID:11373682; http://dx.doi.org/10.1038/35078091
20. Lee A, Zhou H, Scheuer T, Catterall WA. Molecular determinants of Ca^{2+}/calmodulin-dependent regulation of $Ca_V2.1$ channels. Proc Natl Acad Sci U S A 2003; 100:16059-64; PMID:14673106; http://dx.doi.org/10.1073/pnas.2237000100
21. Kim EY, Rumpf CH, Fujiwara Y, Cooley ES, Van Petegem F, Minor DL, Jr. Structures of Ca_V2 Ca^{2+}/CaM-IQ domain complexes reveal binding modes that underlie calcium-dependent inactivation and facilitation. Structure 2008; 16:1455-67; PMID:18940602; http://dx.doi.org/10.1016/j.str.2008.07.010
22. Mori MX, Vander Kooi CW, Leahy DJ, Yue DT. Crystal structure of the Ca_V2 IQ domain in complex with Ca^{2+}/calmodulin: high-resolution mechanistic implications for channel regulation by Ca^{2+}. Structure 2008; 16:607-20; PMID:18400181; http://dx.doi.org/10.1016/j.str.2008.01.011
23. Pate P, Mochca-Morales J, Wu Y, Zhang JZ, Rodney GG, Serysheva, II, Williams BY, Anderson ME, Hamilton SL. Determinants for calmodulin binding on voltage-dependent Ca^{2+} channels. J Biol Chem 2000; 275:39786-92; PMID:11005820; http://dx.doi.org/10.1074/jbc.M007158200
24. Mouton J, Feltz A, Maulet Y. Interactions of calmodulin with two peptides derived from the c-terminal cytoplasmic domain of the $Ca_V1.2$ Ca^{2+} channel provide evidence for a molecular switch involved in Ca^{2+}-induced inactivation. J Biol Chem 2001; 276:22359-67; PMID:11294864; http://dx.doi.org/10.1074/jbc.M100755200
25. Pitt GS, Zuhlke RD, Hudmon A, Schulman H, Reuter H, Tsien RW. Molecular basis of calmodulin tethering and Ca^{2+}-dependent inactivation of L-type Ca^{2+} channels. J Biol Chem 2001; 276:30794-802; PMID:11408490; http://dx.doi.org/10.1074/jbc.M104959200
26. Taiakina V, Boone AN, Fux J, Senatore A, Weber-Adrian D, Guillemette JG, Spafford JD. The calmodulin-binding, short linear motif, NSCaTE is conserved in L-type channel ancestors of vertebrate Cav1.2 and Cav1.3 channels. PLoS One 2013; 8:e61765; PMID:23626724; http://dx.doi.org/10.1371/journal.pone.0061765
27. Liu Z, Vogel HJ. Structural basis for the regulation of L-type voltage-gated calcium channels: interactions between the N-terminal cytoplasmic domain and Ca^{2+}-calmodulin. Front Mol Neurosci 2012; 5:38; PMID:22518098
28. Almagor L, Chomsky-Hecht O, Ben-Mocha A, Hendin-Barak D, Dascal N, Hirsch JA. The role of a voltage-dependent Ca^{2+} channel intracellular linker: a structure-function analysis. J Neurosci 2012; 32:7602-13; PMID:22649239; http://dx.doi.org/10.1523/JNEUROSCI.5727-11.2012
29. Zuhlke RD, Pitt GS, Deisseroth K, Tsien RW, Reuter H. Calmodulin supports both inactivation and facilitation of L-type calcium channels. Nature 1999; 399:159-62; PMID:10335846; http://dx.doi.org/10.1038/20200
30. Zuhlke RD, Pitt GS, Tsien RW, Reuter H. Ca^{2+}-sensitive inactivation and facilitation of L-type Ca^{2+} channels both depend on specific amino acid residues in a consensus calmodulin-binding motif in the a_{1C} subunit. J Biol Chem 2000; 275:21121-9; PMID:10779517; http://dx.doi.org/10.1074/jbc.M002986200
31. Qin N, Olcese R, Bransby M, Lin T, Birnbaumer L. Ca^{2+}-induced inhibition of the cardiac Ca^{2+} channel depends on calmodulin. Proc Natl Acad Sci U S A 1999; 96:2435-8; PMID:10051660; http://dx.doi.org/10.1073/pnas.96.5.2435
32. Kim J, Ghosh S, Nunziato DA, Pitt GS. Identification of the components controlling inactivation of voltage-gated Ca^{2+} channels. Neuron 2004; 41:745-54; PMID:15003174; http://dx.doi.org/10.1016/S0896-6273(04)00081-9
33. Bernatchez G, Talwar D, Parent L. Mutations in the EF-hand motif impair the inactivation of Ba^{2+} currents of the cardiac a_{1C} channel. Biophys J 1998; 75:1727-39; PMID:9746514; http://dx.doi.org/10.1016/S0006-3495(98)77614-3
34. Stephens GJ, Page KM, Bogdanov Y, Dolphin AC. The a_{1B} Ca^{2+} channel amino terminus contributes determinants for b subunit-mediated voltage-dependent inactivation properties. J Physiol 2000; 525 Pt 2:377-90; PMID:10835041; http://dx.doi.org/10.1111/j.1469-7793.2000.t01-1-00377.x
35. Benmocha A, Almagor L, Oz S, Hirsch JA, Dascal N. Characterization of the calmodulin-binding site in the N terminus of $Ca_V1.2$. Channels (Austin) 2009; 3:337-42; PMID:19713738; http://dx.doi.org/10.4161/chan.3.5.9686
36. Brunet S, Scheuer T, Klevit R, Catterall WA. Modulation of $Ca_V1.2$ channels by Mg^{2+} acting at an EF-hand motif in the COOH-terminal domain. J Gen Physiol 2005; 126:311-23; PMID:16157690; http://dx.doi.org/10.1085/jgp.200509333
37. Peterson BZ, DeMaria CD, Adelman JP, Yue DT. Calmodulin is the Ca^{2+} sensor for Ca^{2+}-dependent inactivation of L-type calcium channels. Neuron 1999; 22:549-58; PMID:10197534; http://dx.doi.org/10.1016/S0896-6273(00)80709-6
38. Etzioni A, Siloni S, Chikvashvilli D, Strulovich R, Sachyani D, Regev N, Greitzer-Antes D, Hirsch JA, Lotan I. Regulation of neuronal M-channel gating in an isoform-specific manner: functional interplay between calmodulin and syntaxin 1A. J Neurosci 2011; 31:14158-71; PMID:21976501; http://dx.doi.org/10.1523/JNEUROSCI.2666-11.2011
39. Varnum MD, Zagotta WN. Interdomain interactions underlying activation of cyclic nucleotide-gated channels. Science 1997; 278:110-3; PMID:9311913; http://dx.doi.org/10.1126/science.278.5335.110
40. Trudeau MC, Zagotta WN. Mechanism of calcium/calmodulin inhibition of rod cyclic nucleotide-gated channels. Proc Natl Acad Sci U S A 2002; 99:8424-9; PMID:12048242; http://dx.doi.org/10.1073/pnas.122015999
41. Cens T, Rousset M, Leyris JP, Fesquet P, Charnet P. Voltage- and calcium-dependent inactivation in high voltage-gated Ca^{2+} channels. Prog Biophys Mol Biol 2006; 90:104-17; PMID:16038964; http://dx.doi.org/10.1016/j.pbiomolbio.2005.05.013
42. Grandi E, Morotti S, Ginsburg KS, Severi S, Bers DM. Interplay of voltage and Ca-dependent inactivation of L-type Ca current. Prog Biophys Mol Biol 2010; 103:44-50; PMID:20184915; http://dx.doi.org/10.1016/j.pbiomolbio.2010.02.001
43. Zheng J. Domain-domain interactions in ion channels. J Gen Physiol 2013; 142:347-50; PMID:24043858; http://dx.doi.org/10.1085/jgp.201311090
44. Minor DL, Jr., Findeisen F. Progress in the structural understanding of voltage-gated calcium channel (CaV) function and modulation. Channels (Austin) 2010; 4:459-74; PMID:21139419; http://dx.doi.org/10.4161/chan.4.6.12867
45. Mori MX, Erickson MG, Yue DT. Functional stoichiometry and local enrichment of calmodulin interacting with Ca^{2+} channels. Science 2004; 304:432-5; PMID:15087548; http://dx.doi.org/10.1126/science.1093490

46. Findeisen F, Rumpf CH, Minor DL, Jr. Apo states of calmodulin and CaBP1 control Ca_V1 voltage-gated calcium channel function through direct competition for the IQ domain. J Mol Biol 2013; 425:3217-34; PMID:23811053; http://dx.doi.org/10.1016/j.jmb.2013.06.024
47. Asmara H, Minobe E, Saud ZA, Kameyama M. Interactions of calmodulin with the multiple binding sites of $Ca_V1.2$ Ca^{2+} channels. J Pharmacol Sci 2010; 112:397-404; PMID:20308803; http://dx.doi.org/10.1254/jphs.09342FP
48. Wang C, Chung BC, Yan H, Wang HG, Lee SY, Pitt GS. Structural analyses of Ca^{2+}/CaM interaction with Na_V channel C-termini reveal mechanisms of calcium-dependent regulation. Nat Commun 2014; 5:4896; PMID:25232683; http://dx.doi.org/10.1038/ncomms5896
49. Van Petegem F, Chatelain FC, Minor DL, Jr. Insights into voltage-gated calcium channel regulation from the structure of the $Ca_V1.2$ IQ domain-Ca^{2+}/calmodulin complex. Nat Struct Mol Biol 2005; 12:1108-15; PMID:16299511; http://dx.doi.org/10.1038/nsmb1027
50. Kahanovitch U, Tsemakhovich V, Berlin S, Rubinstein M, Styr B, Castel R, Peleg S, Tabak G, Dessauer CW, Ivanina T, et al. Recruitment of Gβγ controls the basal activity of GIRK channels: crucial role of distal C-terminus of GIRK1. J Physiol London 2014; 592:5373-90; PMID:25384780; http://dx.doi.org/10.1113/jphysiol.2014.283218